

Premature skewing of T cell receptor clonality and delayed memory expansion in HIV-exposed infants

Received: 25 May 2023

Accepted: 15 April 2024

Published online: 14 May 2024

Check for updates

Sonwabile Dzanibe^{1,2}, Aaron J. Wilk³, Susan Canny^{3,4}, Thanmayi Ranganath³, Berenice Alinde⁵, Florian Rubelt^{6,7}, Huang Huang⁷, Mark M. Davis^{6,7,8}, Susan P. Holmes⁹, Heather B. Jaspan^{1,2,10} ✉, Catherine A. Blish^{3,7,11} ✉ & Clive M. Gray^{2,5} ✉

While preventing vertical HIV transmission has been very successful, HIV-exposed uninfected infants (iHEU) experience an elevated risk to infections compared to HIV-unexposed and uninfected infants (iHUU). Here we present a longitudinal multimodal analysis of infant immune ontogeny that highlights the impact of HIV/ARV exposure. Using mass cytometry, we show alterations in T cell memory differentiation between iHEU and iHUU being significant from week 15 of life. The altered memory T cell differentiation in iHEU was preceded by lower TCR V β clonotypic diversity and linked to TCR clonal depletion within the naïve T cell compartment. Compared to iHUU, iHEU had elevated CD56^{lo}CD16^{lo}Perforin⁺CD38⁺CD45RA⁺Fc ϵ R1y⁺ NK cells at 1 month postpartum and whose abundance pre-vaccination were predictive of vaccine-induced pertussis and rotavirus antibody responses post 3 months of life. Collectively, HIV/ARV exposure disrupted the trajectory of innate and adaptive immunity from birth which may underlie relative vulnerability to infections in iHEU.

Early life, especially in Africa, is often plagued by high infectious morbidity with infectious diseases accounting for over two million deaths of which 45% occur during the neonatal period¹. This high mortality rate is most likely linked to the period during which the immune system adapts to extrauterine life. During this transition window, several factors such as maternal morbidity, microbial exposure, and vaccination significantly modulate infant immunity and consequently influences health and disease outcomes^{2–5}. Investigating immune ontogeny and factors that impact immune trajectory during

infancy can provide important insights into understanding how better to combat these early life immune stressors.

Current dogma is that the in-utero environment is sterile and that newborn infants have limited antigen exposure prior to birth, with potentially protective T cells being predominantly naïve and having little T cell receptor (TCR) engagement^{6,7}. This lack of pre-existing adaptive cellular memory early in life is likely to increase the vulnerability of infants to infectious agents and disease, especially if there is an absence of adequate breast-feeding to provide passive maternal

¹Division of Immunology, Department of Pathology, University of Cape Town, Cape Town, South Africa. ²Institute of Infectious Disease and Molecular Medicine, University of Cape Town, Cape Town, South Africa. ³Department of Medicine, School of Medicine, Stanford University, Stanford, CA, USA. ⁴Division of Rheumatology, Department of Pediatrics, Seattle Children's Hospital, Seattle, WA, USA. ⁵Division of Immunology, Department of Biomedical Sciences, Biomedical Research Institute, Stellenbosch University, Cape Town, South Africa. ⁶Department of Microbiology and Immunology, Stanford University School of Medicine, Stanford, CA, USA. ⁷Institute for Immunity, Transplantation and Infection, Stanford University School of Medicine, Stanford, CA, USA. ⁸Howard Hughes Medical Institute, School of Medicine, Stanford University, Stanford, CA, USA. ⁹Department of Statistics, Stanford University, Stanford, CA, USA. ¹⁰Seattle Children's Research Institute and Department of Paediatrics and Global Health, University of Washington, Seattle, WA, USA. ¹¹Chan Zuckerberg Biohub, San Francisco, CA, USA. ✉ e-mail: hbjaspan@gmail.com; cblish@stanford.edu; cgray@sun.ac.za

antibody immunity^{3,8,9}. Since the diversity and composition of T cell immunity is shaped in large part by antigen exposure¹⁰, examining changes in the TCR repertoire during infancy could provide insight into immune development and how disruption of immunity may influence susceptibility to infectious diseases.

The advent of universal treatment with antiretroviral (ARV) drugs to both mother and infant has successfully minimised vertical HIV transmission, but also introduces the possible adverse effect of HIV and ARV exposure on neonatal development *in utero* and in the post-natal period. The intertwined nature of HIV and ARV exposure makes it difficult to unravel, but it is known that HIV/ARV-exposed uninfected infants (iHEU) have higher risk of infectious disease-related morbidity and mortality compared to HIV-unexposed uninfected infants (iHUU) of a similar age, suggesting disruptions to their immune maturation^{11–16}. Many studies investigating immunological disparities between iHEU and iHUU are limited to cross-sectional analysis with few studies investigating longitudinal changes and thus there is a lack of evidence on how T cells mature early in life in the context of HIV/ARV exposure. We have previously shown that maternal HIV/ARV exposure alters the dynamics of the T regulatory (Treg) to Th17 cell ratio resulting in a Th17/Treg imbalance associated with gut damage¹⁷. In this paper, we extend this analysis to investigate the impact of HIV/ARV exposure on T cell clonality, memory and NK cell maturation differences between iHEU and iHUU.

Since early life is also marked by regulated adaptive immunity, neonatal immune defence is heavily reliant on innate immune cells such as NK cells to rapidly eliminate infections. Compared to adults, however, neonatal NK cells display functional defects such as reduced cytolytic activity including antibody mediated cell cytotoxicity^{18,19}, decreased expression of adhesion molecules²⁰ and lower secretion of TNF- α and IFN- γ ²¹. Earlier studies have further demonstrated that compared to iHUU, iHEU have a lower proportion of NK cells measured at birth and at six months and having reduced IFN- γ secretion and perforin expression^{22,23}. In addition, the function of NK cells is influenced by the combinatorial signalling through a diverse array of activating and inhibitory receptors expressed on the cell surface²⁴. The composition of these receptors is driven by past viral exposure^{21,25,26}. Given that NK cells also play a key role in priming the adaptive immune system to respond to invading pathogens or to tailor their immunogenicity towards specific vaccines²⁷, it is important to investigate the maturation trajectory of NK cells in tandem with T cell immune ontogeny. Whether early life exposure to HIV/ARV shapes the maturation and/or diversification of NK cells remains unknown.

Here, we comprehensively investigated the relationship between adaptive and innate immunophenotypes along with TCR diversity and the ability to mount an antibody response to pertussis and rotavirus vaccination. Given the heightened infectious morbidity risk in iHEU, we hypothesised that immune ontogeny is associated with a narrowing TCR repertoire over time in parallel with expanded NK cell subsets in iHEU relative to iHUU. We mapped the immune trajectory of NK and T cell phenotypic clusters in the first 9 months of life and associated this with TCR diversity and antibody titres. Using this approach, we show divergent adaptive immune maturation in iHEU relative to iHUU occurring from 3 months of life with earlier phenotypic differences evident in NK cells. Our data show a narrowing and persistent skewing of the TCR repertoire from birth in iHEU that precedes altered CD4⁺ and CD8⁺ T cell memory development. We also show that specific NK cell clusters at birth can predict the magnitude of pertussis and rotavirus vaccine-induced antibody response and highlights the importance of innate immunity in early life.

Results

Immune cell transition from birth to 9 months of age

Our infant cohort consisted of 36 infants (iHEU=40 and iHUU=16) and having similar population characteristics including birth weight and

gestational age, with the exception that the mothers of iHEU were noted to be significantly older (Table S1). To characterise the immune ontogeny in our infant cohort (Table S1 and Fig. S1), we first analysed the overall immunological trajectories of innate and adaptive immune cells subsets in the first 9 months life. Matched PBMC samples collected at birth and at week 4, 15 and 36 as well as some matching cord blood mononuclear cells were analysed for immunophenotypic changes using a mass cytometry antibody panel (Table S2).

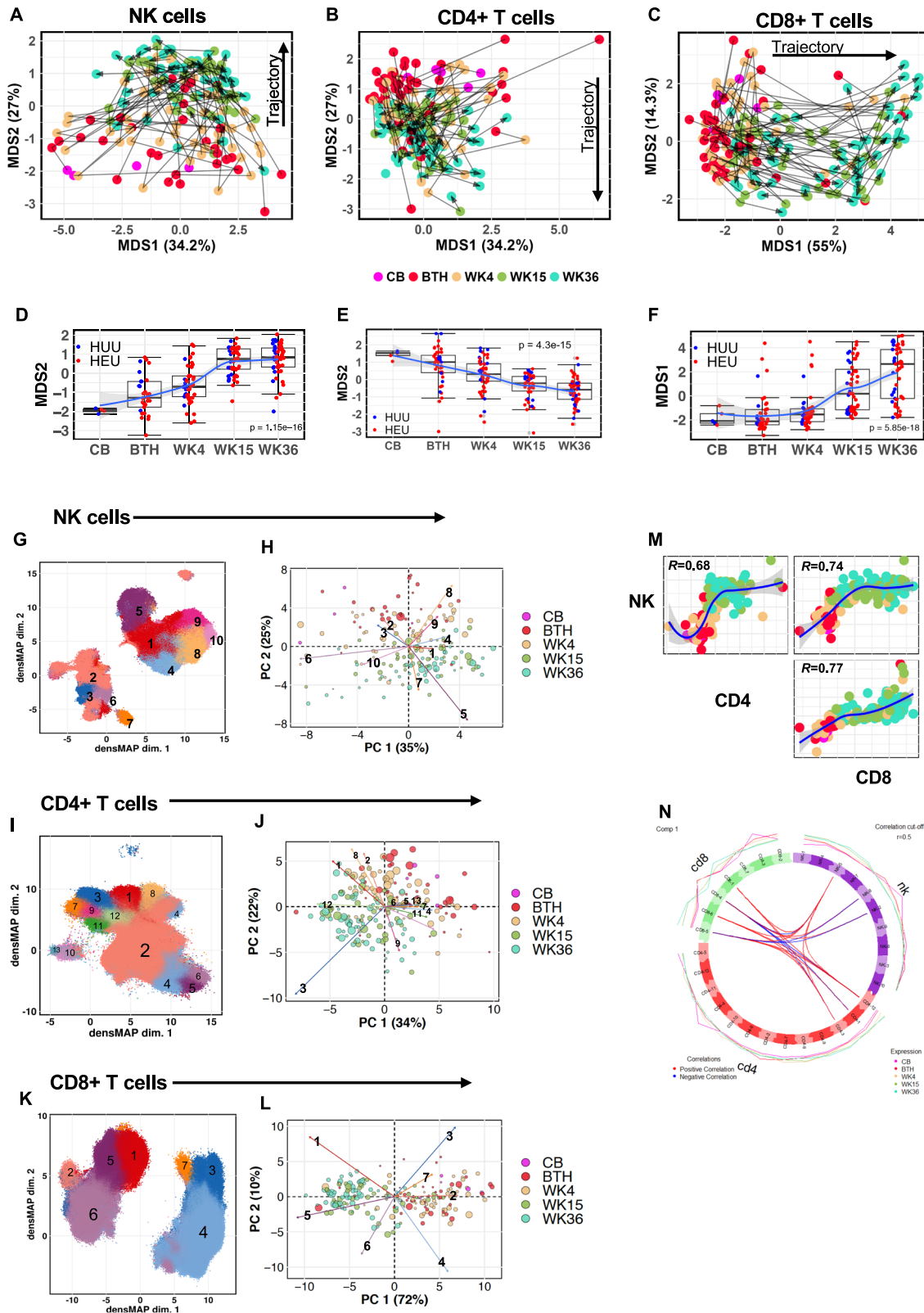
Unsupervised cell clustering using the live singlet cell population (Fig. S2A) from all infant samples was used to describe the trajectories of myeloid and lymphoid lineages in infants. Using this approach, we could identify 11 cell clusters (Fig. S2B and S2C), consisting of B cells (cluster 1), T cells (CD4⁺ T cluster 2 and CD8⁺ T clusters 3, 4, and 9), monocytes (cluster 8), NK cells (cluster 10), and NKT-like cell (cluster 11). The three CD8⁺ T cell clusters (3, 4 and 9) were delineated as naïve (13.9%, CD45RA⁺CD27⁺CCR7⁺), a small effector memory population (0.07%, EM: CD45RA⁺CD27⁺CCR7) and effector cells (4.4%, Eff: CD45RA⁺CD27⁺CCR7). We also identified a lineage negative cluster (3.2%) and one monocyte-like cluster expressing HLA-DR only (1.2%). Although we employed computational doublet removal from our clustering analysis, a minor miscellaneous population (0.65%) co-expressing typically mutually exclusive lineage markers was identified (Fig. S1A and S1B). This small population is shown as a central cluster 7 in the dimensional reduction of the immune cell clusters (Fig. S2C) and was excluded from downstream analysis.

When we examined the remaining clusters over time, we observed an age dependent segregation of cells. The proportions of cell clusters changed over 36 weeks of life, where monocytes ($\rho = -0.4$, $p < 0.001$) and CD4⁺ T cells ($\rho = -0.36$, $p < 0.001$) diminished with age, B cells ($\rho = 0.66$) and effector memory CD8⁺ T cells ($\rho = 0.54$) were positively correlated to infant age (Fig. S2D and S2E).

Distinct temporal maturation trajectories of NK cells stabilising at 4 months coinciding with rapid CD8⁺ T cell divergence

Since our mass cytometry antibody panel (Table S2) was mainly focused on assessing ontological changes of NK cells and T cells, we then manually gated on CD4⁺ and CD8⁺ T cells from the CD3⁺ T cell population and targeted the NK cell population using lineage-exclusion manual gating (Fig. S2A). The median marker expression for each sample was used to compute multidimensional scaling (MDS) coordinates, which revealed that intra-individual variability amongst the infants was associated with age (Fig. 1A–F). The grouping of the samples by marker expression displayed a converging trajectory along the MDS2-axis for NK cells although stabilizing from week 15 (Fig. 1D). The CD4⁺ displayed a gradual maturation transition from birth to week 36, consistent with previous findings showing neonatal to adult immunological transition²⁸. CD8⁺ T cells, however, revealed a divergent trajectory along the MDS1-axis (Fig. 1D), with a significant expansion by week 15 (Fig. 1E).

We then proceeded to identify the maturation trajectories of the different subsets within each cell population by performing unsupervised cell clustering based on marker expressions. Across all time points, we could identify 10 NK cell clusters, 13 CD4⁺ T cells and 7 CD8⁺ T cells. (Fig. 1G–L, Tables 1–3 and Fig. S3). Principal Component Analysis (PCA) using centred log-ratios of the relative cluster abundances for each sample also demonstrated grouping of the infants by their respective age (Fig. 1H, J, L). NK cell cluster 8 (CD56⁺CD16⁺NKG2A⁺CD45RA⁺Perforin⁺) was more abundant at earlier time points (birth and week 4), while cluster 5 (CD56⁺CD16⁺CD57⁺CD45RA⁺Perforin⁺) was significantly abundant at later time points (week 15 and 36) demonstrating a typical NK cell maturation trajectory (Figs. 1H and S3A). Similarly for T cell populations, CD4⁺ and CD8⁺ clusters reflected the immunological trajectory shown in Fig. 1B, C, with the terminally differentiated clusters: CD4⁺ cluster 3 (CD45RA⁺CD57⁺Perforin⁺PD-1⁺) and CD8⁺ clusters 1



(CD45RA⁺CD57⁺Perforin⁺CCR4⁺) and 5 (CD45RA⁺CD57⁺Perforin⁺) increasing with infant age (Fig. 1I–L, S3B and S3C).

We further interrogated the compositional relationship amongst the different cell clusters by integrating the 3 data sets derived from NK cells and CD4⁺ and CD8⁺ T cells and performed a block partial least square regression with discriminant analysis using DIABLO (Data Integration Analysis for Biomarker discovery using Latent

cOmponents)²⁹. Using this analytical approach, we could observe the strong correlation between the maturation of CD4⁺ and CD8⁺ T cells with advancing infant age (Spearman's rank correlation, Fig. 1M). Moreover, the converging maturation trajectory of NK cells, which stabilised at week 15, coincided with the rapid expansion of CD8⁺ T cells (Fig. 1M). This suggests maturational regulation between the cytolytic cells during the neonatal - infant transition as demonstrated

Fig. 1 | Immunophenotypic trajectory of infant NK cells and T cells in the first 9 months of life. A–C Age related maturation trajectory of NK cells and CD4⁺ and CD8⁺ T cells depicted using multidimensional scaling (MDS) coordinates derived from median marker expressions for each infant samples collected in cord blood (CB, *n* = 5) and at birth (BTH, *n* = 44) and weeks (WK) 4 (*n* = 53), 15 (*n* = 52) and 36 (*n* = 53). **D–F** Boxplots summarising MDS coordinate associated with infant age for NK cells and CD4⁺ and CD8⁺ T cells. Boxplot central line depicts the median, the upper and lower lines represents the 75th and 25th percentile respectively, and the whiskers mark the 1.5 times the 75th and 25th percentile boundary, (*p* = Kruskal Wallis). Summary trendline shows local regression as determined by local estimated scatterplot smoothing (LOESS) with 95%CI error bands. **G, I, K** Uniform

manifold approximation and proximation (UMAP) with density preservation showing dimensional reduction of FlowSOM clusters of NK cells and CD4⁺ and CD8⁺ T cells, respectively. **H, J, L** Age related phenotypic composition of NK cells and CD4⁺ and CD8⁺ T cells depicted as principal component (PC) coordinates of centred log-odd ratios of the FlowSOM clusters for each infant samples and arrows indicating contribution of each cell cluster in the scatter of PC components. **M** Spearman's correlation of PC coordinates associated with immune trajectory for NK cells, and CD4⁺ and CD8⁺ T cells. Summary trendline shows local regression as determined by LOESS with 95%CI error bands. **N** Circoplot showing correlations among immune cell clusters derived from NK cells, and CD4⁺ and CD8⁺ T cells.

by the negative correlation between NK cell cluster 8 (Perforin⁺CD38⁺NKG2A⁺Nkp30⁺Nkp46⁺Siglec-7⁺FcεR1γ⁺) and CD8⁺ T cell cluster 5 (Perforin⁺CD57⁺CD45RA⁺DNAM1⁺LILRB1⁺2B4⁺), while CD8⁺ T cell cluster 5 was positively correlated to NK cell cluster 5 (Perforin⁺CD45RA⁺CD38⁺FcεR1γ⁺LILRB + CD57⁺).

Overall, these temporal phenotypic changes in cell clustering illustrate the archetypal progression and transition of infant immunity from neonatal to an adult-like immune phenotype by 9 months of age, being characterised by a shift from innate myeloid cells to an increase in lymphoid adaptive immune cells³⁰.

Memory maturation of CD4 and CD8 T cells is disrupted by HIV exposure after three months of life

In our previous analysis we observed altered expansion of T regulatory cells among iHEU relative to iHUU counterparts¹⁷. We were thus interested in determining the extent of maternal HIV infection in modulating the trajectory of infant immune maturation. PCA components derived from the centred log-ratios of the relative cluster abundances for each cell subsets were compared between iHEU and iHUU to determine compositional differences. There were statistically significant differences at weeks 15 and 36 for CD4⁺ T cells and at week 36 for CD8⁺ T cells (Fig. 2B, C). Differential abundance testing using generalised linear mixed model revealed that the divergent CD4⁺ T cell phenotypes in iHEU were due to lower frequencies of closely related activated and proliferating (HLA-DR⁺Ki67⁺) clusters 4 & 11, and memory differentiated cytolytic (PD-1⁺CD57⁺Perforin⁺)^{31,32} clusters 5-9 compared to iHUU at week 15, with the differentiated cytolytic clusters 5, 7 and 9 remaining significantly lower in iHEU at week 36 (Fig. 2D, E). The CD4⁺ Th2-like cluster 1 (CCR4⁺CD27⁺CD127⁺) was, however, significantly higher in iHEU compared to iHUU at week 15 although by week 36 was no longer significantly elevated (Fig. 2D, E). We further noted that the proportion of Th2-like cluster was also higher in iHEU

compared to iHUU at week 4, albeit not significant following correction for multiple comparisons (Fig. S4A).

For CD8⁺ T cells, the compositional differences were partly driven by lower mean frequencies for clusters 2 (NKT-like cells: CD56^{lo}CD16⁺Nkp30⁺Nkp46⁺NKG2A⁺Perforin⁺)³³, 3 (Naïve-like activated cell: CD45RA⁺CD27⁺CCR7⁺CXCR3⁺CCR4⁺HLA-DR⁺) and 7 (proliferating EM: Ki67⁺CD45RA⁺CD27⁺CCR7⁺Perforin⁺) in iHEU compared to iHUU at week 15 (Fig. 2I). By week 36, only the mean frequencies of clusters 2 (NKT-like cells) and 3 (Naïve-like cells) remained significantly lower in iHEU compared to iHUU (Fig. 2F, G).

The composition of NK cells differed by HIV-exposure only at week 4 (Fig. 2A), partly driven by higher frequencies of the differentiated (CD56^{lo}NKG2A⁺CD57^{lo/+})³⁴ NK cell cluster 1 (CD56^{lo}CD16^{lo}Perforin⁺CD38⁺CD45RA⁺FcεR1γ⁺, *p* = 0.04, *p*.adj = 0.2) and cluster 5 (CD56^{lo}CD16⁺Perforin⁺CD57⁺CD45RA⁺CD38⁺) (*p* = 0.03, *p*.adj = 0.2) in iHEU compared to iHUU (Fig. S4B), although these difference were not significant after correcting for multiple testing.

These findings show that HIV/ARV exposure sequentially disrupts immune trajectory over time after birth beginning with subtle changes in innate NK cells and delaying memory T cell maturation.

Early T Cell Receptor repertoire skewing in iHEU

To relate altered T cell memory maturation trajectories to T cell repertoire changes, we characterised TCRβ clonotypes in sorted naïve and memory T cells from matching samples used to define memory lineage in our CyTOF panel (Fig. S1). Each PBMC sample was sorted into four T cell subsets: naïve (CD45RA⁺CD27⁺CCR7⁺) CD4⁺ and CD8⁺ cells and total memory (CD45RA^{+/−}CD27^{+/−}CCR7^{+/−}) T cells (Fig. S5A and Data S1). The sorted cell fractions were subjected to bulk sequencing of the TCR Vβ locus which enabled identification of TCR clones in 885 samples. There were 24 samples that had either fewer than 10 clones or the number of unique clones were greater than the number of cells sequenced, and these were removed from downstream analysis (Fig. S1). Of the remaining 861 samples included in the study analysis, there was a total of 238,092 reads (range: 11-5451), which differed between iHEU and iHUU for naïve CD4⁺ T cells at weeks 36 (Data S1). The number of unique clones identified per T cell subset positively correlated with the total number of reads (Fig. S5B). The median number of unique clones per T cell subset, however, was higher in memory T cells for iHUU compared to those of iHEU at birth, and for naïve CD4⁺ T cell a similar difference was observed at week 36 (Data S1). CDR3 lengths of the clonotypes were evenly distributed across infant age and between iHEU and iHUU (Fig. S5C).

We assessed the TCRβ repertoire during infancy by calculating the inverse Simpson diversity index and Chao1 richness scores and noted that the overall TCRβ repertoire remained relatively stable over the first 9 months (Fig. S5D and S5E). However, when the TCRβ diversity scores were stratified by infant HIV exposure status, the TCRβ diversity for iHUU memory CD4⁺ T cells significantly decreased over time (*p* = 0.032, Fig. S6A). Moreover, iHEU memory TCRβ clonotypes had relatively lower diversity compared to iHUU at birth (Fig. 3A). Similarly, richness (the number of unique TCRβ clones) was significantly lower in

Table 1 | Phenotypic description of NK cell clusters identified by unsupervised cell clustering

Cluster	Phenotype	(%)
(1)	(CD56 ^{lo} CD16 ^{lo}) Perforin ⁺ CD38 ⁺ CD45RA ⁺ FcεR1γ ⁺	30.5
(2)	(CD56 ^{lo} CD16 ⁺) DNAM1 ⁺	20.7
(3)	(CD56 ^{lo} CD16 ⁺) FcεR1γ ⁺	1.8
(4)	(CD56 ^{lo} CD16 ⁺) Perforin ⁺ CD45RA ⁺ CD38 ⁺ 2B4 ⁺ FcεR1γ ⁺	11.7
(5)	(CD56 ^{lo} CD16 ⁺) Perforin ⁺ CD45RA ⁺ CD38 ⁺ FcεR1γ ⁺ LILRB ⁺ CD57 ⁺	12.4
(6)	(CD56 ^{lo} CD16 ^{lo}) FcεR1γ ⁺ DNAM1 ⁺ HLA-DR ⁺ CXCR3 ⁺ CCR4 ⁺	1.4
(7)	(CD56 ^{lo} CD16 ⁺) CD38 ⁺ CD39 ⁺ CD27 ⁺ Ki67 ⁺	0.9
(8)	(CD56 ^{lo} CD16 ⁺) Perforin ⁺ CD38 ⁺ CD45RA ⁺ DNAM1 ⁺ 2B4 ⁺ Nkp30 ⁺ Nkp46 ⁺ NKG2A ⁺ Siglec-7 ⁺ FcεR1γ ⁺	15.0
(9)	(CD56 ^{br} CD16 ⁺) DNAM1 ⁺ NKG2D ⁺ Nkp46 ⁺ NKG2A ⁺	4.9
(10)	(CD56 ^{lo} CD16 ⁺) Perforin ⁺ CD38 ⁺ CD45RA ⁺ LILRB1 ⁺ NTBA ⁺ 2B4 ⁺ Nk30 ⁺ NKG2D ⁺ HLA-DR ⁺ CCR4 ⁺ CCR7 ⁺ PD-1 ⁺ TIGIT ⁺ NKG2C ⁺	0.7

Table 2 | Phenotypic description of CD4⁺ T cell clusters identified by unsupervised cell clustering

Cluster	Phenotype	(%)
(1)	CCR4+ CD27+ CD127+ (Th2)	5.07
(2)	CD38+ CD45RA+ CD27+ CCR7+ CD127+ (Naïve)	84.1
(3)	CD45RA+ CD57+ Perforin+ PD-1+ (Cytotoxic TD)	1.3
(4)	CD38+ HLA-DR+ CD45RA+ CD27+ CCR7+ (Activated cells)	4.7
(5)	CD27+ CD38+ CD45RA+ CCR7+ CCR4+ CCR6+ CXCR3+ TIGIT+ PD-1+ HLA-DR+ CD69+ (Th1/17 Activated)	0.7
(6)	CD27+ CD38+ CD45RA+ CCR7+ CCR4+ CCR6+ CXCR3+ TIGIT+ PD-1+ CD57+ CD39+ (Th1/Th17)	0.2
(7)	CD27+ Perforin+ CD45RA+ CCR7+ CD38+ TIGIT+ Ki67+	0.3
(8)	CD25+ CD39+ TIGIT+ CCR4+ PD-1+ (Treg cells)	0.9
(9)	CD27+ CD38+ CD45RA+ CCR7+ Perforin+ Ki67+ CD25+	0.3
(10)	CD27+ CD38+ CD45RA+ CCR7+ Perforin+ Ki67+ HLA-DR+ CD69+ CD39+	0.1
(11)	Perforin+ Ki67+ CD27+ CD38+ CD45RA+ CCR7+ CD127+	0.2
(12)	CD27+ PD-1+ CD38+	2.07
(13)	CD39+ CD45RA+	0.1

Table 3 | Phenotypic description of CD8⁺ T cell clusters identified by unsupervised cell clustering

Cluster	Phenotype	(%)
(1)	Perforin+ CD45RA+ CD38+ HLA-DR+ CCR4+ Siglec-7+ CD57+ (TD)	7.5
(2)	CD56+ CD16+ Perforin+ FcεR1γ+ NkpK6+ NKG2A+ (NKT-like)	0.4
(3)	CD45RA+ CD27+ CCR7+ CD127+ HLA-DR+ CXCR3+ CD38+	2.7
(4)	CD45RA+ CD27+ CCR7+ CD127+ CD38+ (Naïve)	55.3
(5)	Perforin+ CD57+ CD45RA+ DNAM1+ LILRB1+ 2B4+	15.6
(6)	Perforin+ CD38+ 2B4+ NTB4+	18.4
(7)	Ki67+ CD45RA+ CD27+ Nkp30+ KIR2DL1+	0.1

iHEU relative to iHUU for both memory CD4⁺ and CD8⁺ T cells at birth (Fig. 3B). This remained statistically significant for memory CD4⁺ T cells at week 4 (Fig. 3B).

In contrast to TCRβ of memory T cells, in which significant differences were found early life, within the naïve T cell compartment; TCRβ diversity was significantly lower in iHEU compared to iHUU at week 15 and 36 for CD4⁺ T cells, and at birth and week 36 for CD8⁺ T cells (Fig. 3A). Significant differences in TCRβ richness for naïve T cells were partially complementary to the differences observed for TCRβ diversity, being lower in iHEU compared to iHUU at birth and week 36 for CD4⁺ T cells and only at birth for CD8⁺ T cells (Fig. 3B).

We also observed differences in the overall structural overlap, as measured by Jaccard indices, of the memory CD4⁺ TCR repertoire between iHEU and iHUU at birth, although this difference was less prominent at later time points (Fig. S6B). In contrast, the TCRβ structural overlap for naïve CD8⁺ T cells was lower in iHEU compared to iHUU only at week 36 (Fig. S6B). Differences in Vβ gene usage were observed between iHEU and iHUU with most genes being used more frequently in iHEU (Fig. S6C). Together, these results suggest expansion of specific TCR clones among iHEU, resulting in skewing of the TCRβ repertoire relative to iHUU and which likely occurred *in utero*.

Since the naïve TCRβ clonotypic differences coincided with the lower memory differentiated T cell clusters (Fig. 2), we next wished to determine if there was a relationship between TCRβ diversity and the clusters of CD4⁺ and CD8⁺ T cells identified. Spearman's rank correlation between T cell clusters and the inverse Simpson TCRβ diversity scores for naïve and memory CD4⁺ and CD8⁺ T cells were measured for infants with paired TCRβ and mass cytometry data at all time points.

Here, the TCRβ diversity scores derived from sorted naïve T cells in iHEU were positively correlated to the frequencies of CD4⁺ T cell clusters (4–6, 9–11) and CD8⁺ T cell clusters (2,3,7) (Fig. 3C).

It is noteworthy that the observed T cell clusters that were correlated to the naïve TCRβ diversity included the HLA-DR⁺Ki67⁺CD4⁺ T cell clusters (4 & 11), memory differentiated CD4⁺ T cell clusters (5,6, 9 & 11) and the CD8⁺ T cell clusters (2,3 & 7) that were significantly lower amongst iHEU at week 15 and 36 (Fig. 2D–G). Relative to the naïve CD4⁺ and CD8⁺ T cell clusters, the T cell clusters that were correlated with TCRβ displayed varying expression levels of PD-1 suggesting TCR activation (Fig. S3B and S3C)^{35,36}. For the proliferating activated CD4⁺ T cells (cluster 4 & 11) and the terminally differentiated cytolytic CD4⁺ T cells (cluster 5 & 6), these correlations were evident from birth up until week 15. Although a similar trend was observed for the T cell clusters and TCR diversity derived from sorted memory T cells, the observed correlations were not statistically significant after correcting for multiple comparisons (Fig. S6D).

Collectively, our findings show skewing of the TCR repertoire in iHEU relative to iHUU from birth and the early increased T cell clonality preceding T cell memory differentiation was a hallmark finding of HIV/ARV exposure.

Predicted TCR recognition of epitopes found only in iHUU

To understand the predicted antigen specificities of the TCR clonotype differences between iHEU and iHUU, we used GLIPH2 (grouping of lymphocyte interactions by paratope hotspots)^{37,38}. TCR specificities from sorted naïve CD4⁺ T cells in iHUU appeared enriched with specificities for cytomegalovirus (CMV), Hepatitis C virus (HCV), SARS-Cov2 and HIV-1 (Fig. 3D). Enrichment of Influenzae A specific clones was more apparent in memory CD4⁺ T cells at the week 36. For memory CD4⁺ T cells at week 4, the shared specificity groups in iHUU were enriched for CMV clones. Similarly, for CD8⁺ T cells, there were more specificities in the naïve compartment at both earlier and later time points with less predictions in memory CD8⁺ T cells. TCR specificities in sorted naïve CD4⁺ and CD8⁺ cells from iHUU appeared consistent throughout 36 weeks, whereas specificities in the CD4⁺ T cell memory compartment fluctuated and appeared predominantly at 4 and 36 weeks (Fig. 3D). Conversely for iHEU sorted T cell populations, no enriched TCR specificities in either naïve or memory CD4⁺ or CD8⁺ cells at any of the time points were predicted.

NK cell clusters are the strongest predictors of antibody responses

To relate how early life NK cell and T cell clusters associate with functional immune outcomes in infants included in this study, antibody responses were measured against acellular pertussis vaccination from birth to 36 weeks and to rotavirus at 36 weeks in matching infants used for immunophenotyping by mass cytometry (Fig. S1). We initially hypothesised that iHEU would have lower IgG and IgA responses compared with iHUU after vaccination with routine administration of these vaccines, which may explain a mechanism for higher infection rates among iHEU. The median anti-pertussis IgG titres were lower in iHEU compared to iHUU at birth and at week 4 (pre-vaccination; Fig. 4A). However, at week 15 (1 week post 3rd vaccine dose), iHEU showed a significantly higher anti-pertussis IgG response relative to iHUU, persisting until week 36 (Fig. 4A). No significant differences were observed in anti-rotaviral IgA levels or ability to neutralise rotavirus between iHEU and iHUU (Figs. 4B and S7A).

To determine contemporaneous cell clusters that were related to these antibody responses, we correlated the frequencies of cell clusters at weeks 15 and 36 with anti-pertussis IgG and anti-rotavirus IgA titres. CD4⁺ T cell cluster 1 (Th2-like cells) associated with antibody production³⁹, was significantly correlated to pertussis antibody titres at week 15 ($\rho = 0.44$, $p_{\text{adj}} = 0.048$; Fig. 4C). Although a similar trend was observed for both iHEU and iHUU, these correlations were not

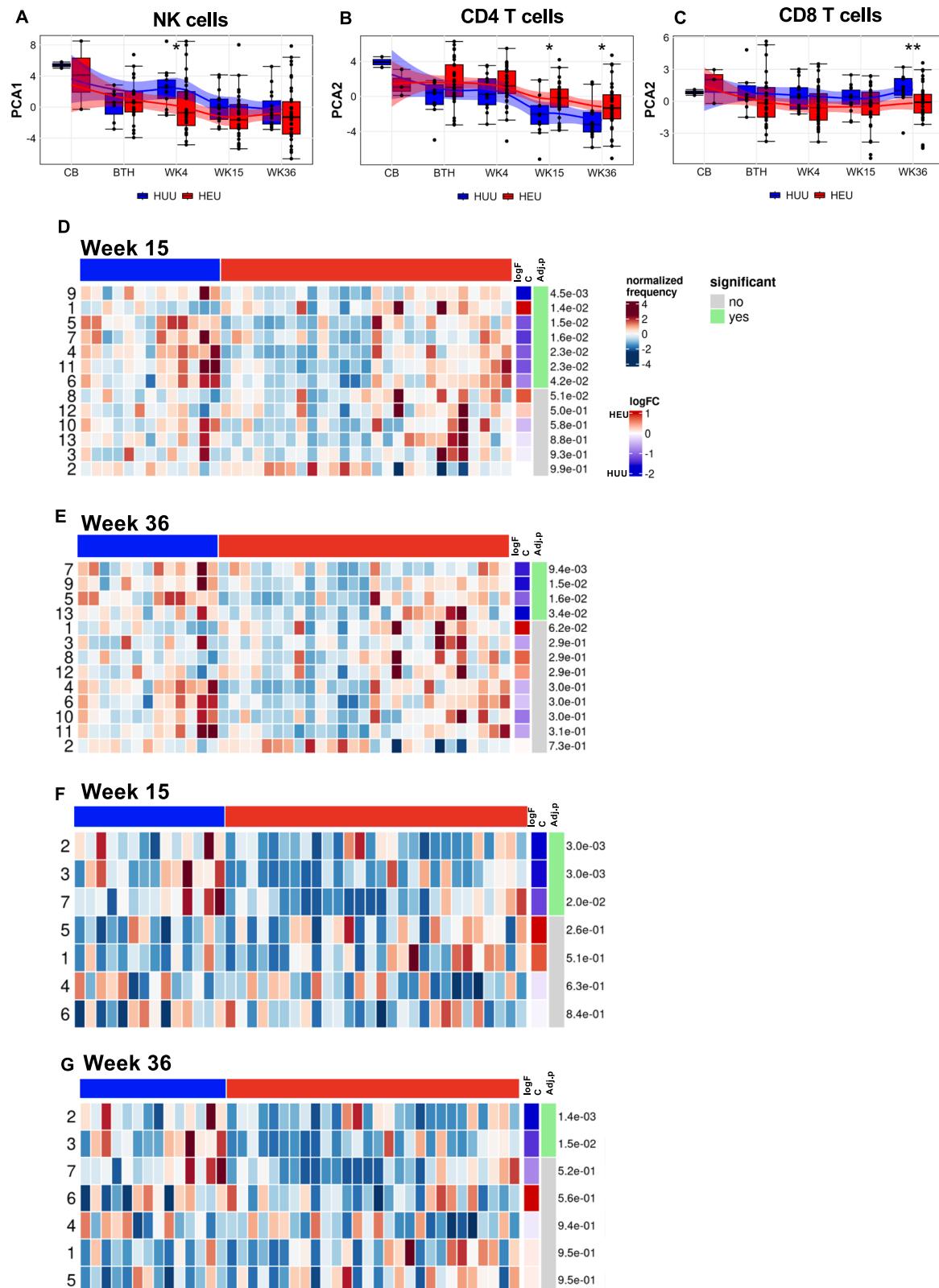


Fig. 2 | Divergent T cell memory differentiation in HIV-exposed uninfected infants (iHEU) compared to HIV-unexposed uninfected infants (iHUU).

A–C Boxplots comparing PC coordinates derived from centred log-odd ratios of FlowSOM NK cell, and CD4⁺ and CD8⁺ T clusters between iHEU and iHUU at birth (BTH), weeks (WK) 4, 15 and 36. Boxplot central line depicts the median, the upper and lower lines represents the 75th and 25th percentile respectively, and the whiskers mark the 1.5 times the 75th and 25th percentile boundary (* $p < 0.05$, ** $p < 0.01$; Two-sided Wilcoxon). Summary trendline shows local regression as

determined by local estimated scatterplot smoothing (LOESS) with 95%CI error bands. D, E Generalised linear mixed model (GLMM) comparing the abundances of CD4⁺ T cell clusters between iHEU and iHUU at weeks 15 and 36. F, G GLMM comparing the abundances of CD8⁺ T cell clusters between iHEU and iHUU at weeks 15 and 36. Positive log Fold change (FC) signified cell cluster frequencies were higher in iHEU compared to iHUU. False discovery rate (FDR) was used to correct for multiple comparison and adjusted p values are presented.

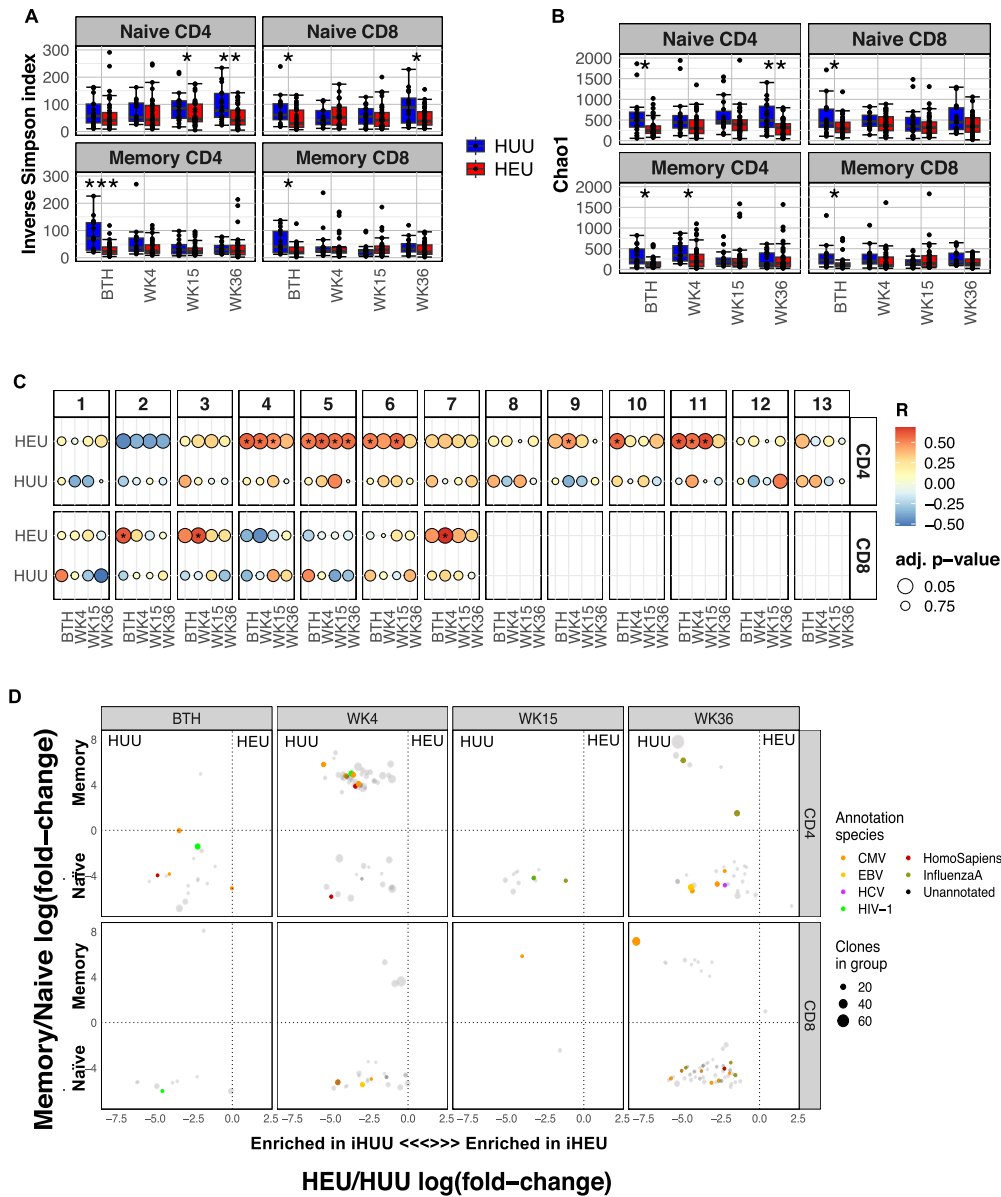


Fig. 3 | Premature CD4+ and CD8+ T cell receptor (TCR) repertoire skewing in HIV-exposed uninfected infants (iHEU) relative to HIV-unexposed uninfected infants (iHUU). **A** Boxplots comparing Inverse Simpson TCR diversity scores between iHUU and iHEU at birth (BTH) and weeks (WK) 4, 15 and 36. **B** Boxplots comparing Chao1 TCR clonotype richness between iHUU and iHEU at BTH and WK4, 15 and 36. All boxplots used the standard Tukey's representation with the central line depicting the median, the upper and lower lines represent the 75th and 25th percentile respectively, and the whiskers mark the boundary at 1.5 times of the

75th and 25th percentile ($*p < 0.05$, $**p < 0.01$ and $***p < 0.001$; Two-sided Wilcoxon). **C** Spearman's rank correlation between naive CD4⁺ and CD8⁺ T cell Inverse Simpson scores and frequencies of CD4⁺ and CD8⁺ T cell clusters respectively. $*adjusted\ p < 0.05$, FDR used to correct for multiple comparisons. **D** GLIPH analysis showing antigen specificity that were significantly enriched in iHUU relative to iHEU and in naïve relative to memory CD4⁺ and CD8⁺ T cell subsets. Sample size for each group is shown in Fig. S1.

statistically significant after adjusting for multiple comparisons (Fig. S7B). At week 36, there was an inverse correlation between pertussis antibody levels and CD4⁺ T cell cluster 11 (HLA-DR⁺Ki67⁺), terminally differentiated clusters 6,7, and 9 (PD-1 + CD57+Perforin +), and clusters 10 and 13 (CD38⁺CD39⁺), and also the CD8⁺ T cell cluster 7 (Proliferating EM: Ki67⁺CD45RA⁺CD27⁺CCR7⁺). Of note, there was no significant contemporaneous correlation between the NK cell clusters and pertussis antibody titres (Figs. 4C and S7B). In addition, the levels of anti-rotavirus IgA at week 36 were not correlated to any of the identified NK cell and T cell clusters (Fig. 4D).

We next assessed whether immune cell compositions at birth could predict vaccine outcomes during infancy. We built a prediction model by grouping all infants (iHEU and iHUU) into those that had a

positive pertussis-specific IgG titre ($\geq 0.469\ OD_{Abs}$) denoted as responders and those that were non-responders ($< 0.469\ OD_{Abs}$). Most of the infants at birth and week 4 (89.7% and 94.1%, respectively) were determined to be non-responders as expected, since this was prior to vaccination. At week 15 and 36 of age, 46.4% and 34.0% infants respectively were determined to be responders (Fig. 4A).

Multivariate unbiased variable selection using MUV^{R40} was performed to determine early life immune composition that could distinguish later pertussis vaccine responders from non-responders. The abundances of cell clusters with low misclassification MUV^R scores of pertussis vaccine response at weeks 15 and 36 (Fig. S8), were then used to perform a partial least squares discriminant analysis (PLS-DA) with the pertussis IgG titres at week 15 and 36 as response variables. The

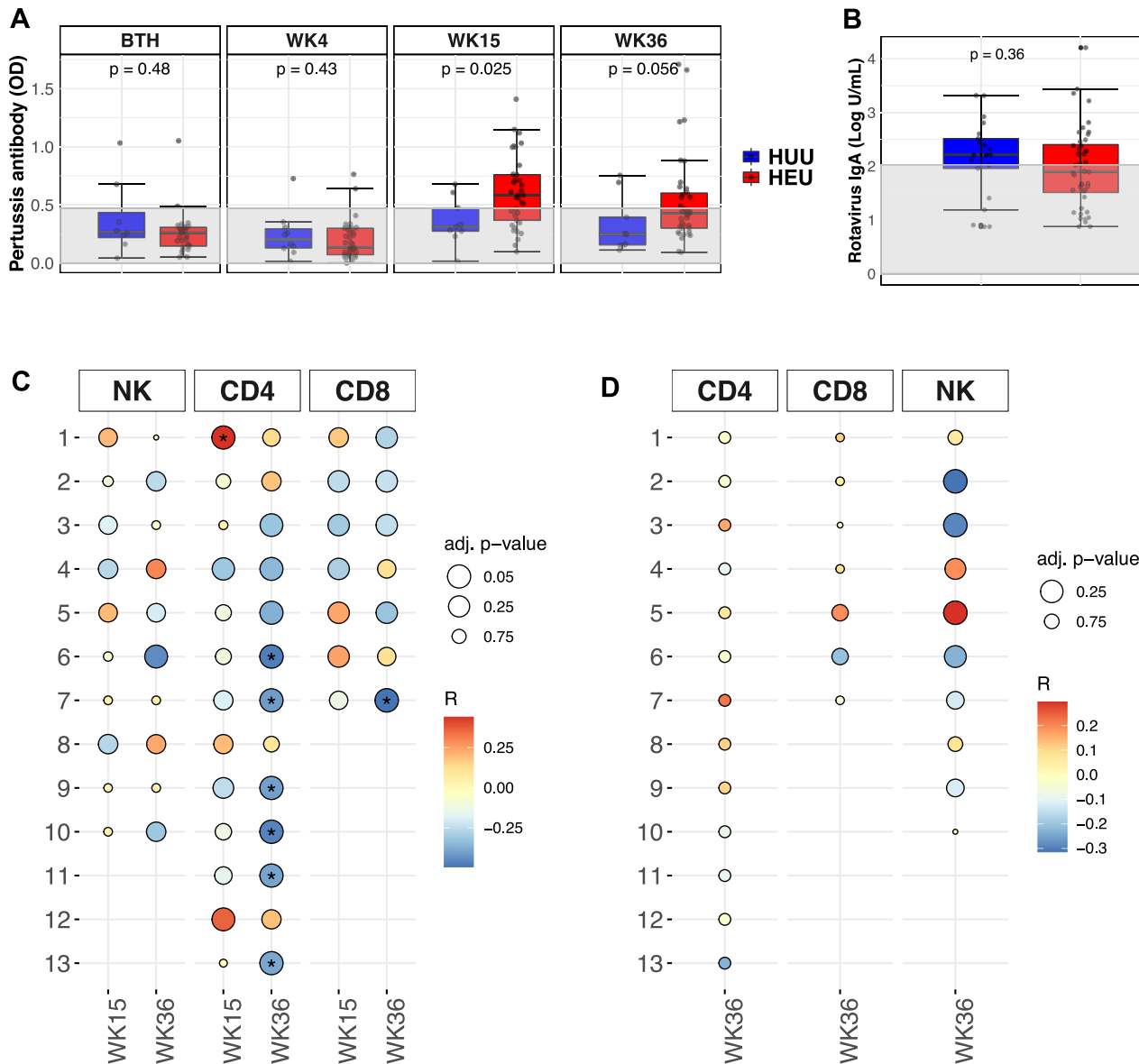


Fig. 4 | Association of vaccine antibody responses to immune cell phenotypes.

A Comparing IgG levels against pertussis between HIV-exposed uninfected infants (iHEU) and HIV-unexposed uninfected infants (iHUU), grey shaded area indicate threshold IgG levels for protective pertussis vaccine response. **B** Boxplots comparing rotavirus specific IgA titres between iHEU and iHUU at week 36. All boxplots used the standard Tukey's representation with the central line depicting the

median, the upper and lower lines represent the 75th and 25th percentile respectively (* $p < 0.05$, ** $p < 0.01$ and *** $p < 0.001$; Two-sided Wilcoxon). **C, D** Spearman's correlation of FlowSOM clusters abundances for NK cells, CD4⁺ and CD8⁺ T cells to anti-pertussis IgG and anti-rotavirus IgA respectively measured at week 15 and 36. *adjusted $p < 0.05$, FDR used to correct for multiple comparisons.

latent variables (LV) of the cell clusters as determined by PLS-DA were then used to compute area under the curve (AUC) of the receiver operating curve (ROC) distinguishing pertussis responders from non-responders (Figs. 5A and S7C). This approach revealed that compared to T cells, the NK cell cluster compositions at birth and at week 4 were superior predictors of the pertussis IgG vaccine response at week 15 (Fig. 5A, at birth: AUC = 0.93 and $p = 0.005$; at week 4: AUC = 0.89 and $p = 0.0003$). NK cell cluster 1 (CD56^{lo}CD16^{lo} Perforin⁺CD38⁺CD45RA⁺FcεRIγ⁺) and cluster 3 (CD56^{lo}CD16^{lo} Perforin⁺CD38⁺CD45RA⁺DNAMI1⁺2B4⁺Nkp30⁺Nkp46⁺NK-NKG2A⁺Siglec-7⁺FcεRIγ⁺) was associated with non-responders to pertussis vaccine (Fig. 5B).

The cell clusters derived from CD4⁺ or CD8⁺ T cells were not predictive of IgG pertussis vaccine response at weeks 15 and 36

(Fig. 4D and S7C), for CD4 clusters at birth: AUC = 0.73, $p = 0.064$; for CD8 clusters: AUC = 0.69, $p = 0.12$; at week 4: CD4 clusters AUC = 0.70, $p = 0.055$; CD8 clusters AUC = 0.70, $p = 0.053$.

Using the same approach for rotavirus responses, we used an arbitrary threshold of overall median concentrations for IgA responses to dichotomize infants into those that had concentrations below the median (low-responders) and those above the median (high-responders; Fig. 4B). In iHUU, 66.7% were high rotavirus vaccine responders compared to 45.5% iHEU ($p = 0.11$). We subsequently determined which immune cell clusters at birth and week 4 were predictive of IgA responses measured at week 36 using MUVr (Fig. S9). PLS-DA analysis using the MUVr selected cell clusters revealed that NK cells at birth were highly predictive of an IgA rotavirus response at week 36 (Fig. 5C, AUC = 0.92, $p = 0.0007$). Similar to the anti-pertussis response, NK cell cluster 1 was also associated with high anti-rotavirus IgA responses, while NK cell cluster 8 was associated with low anti-rotavirus IgA

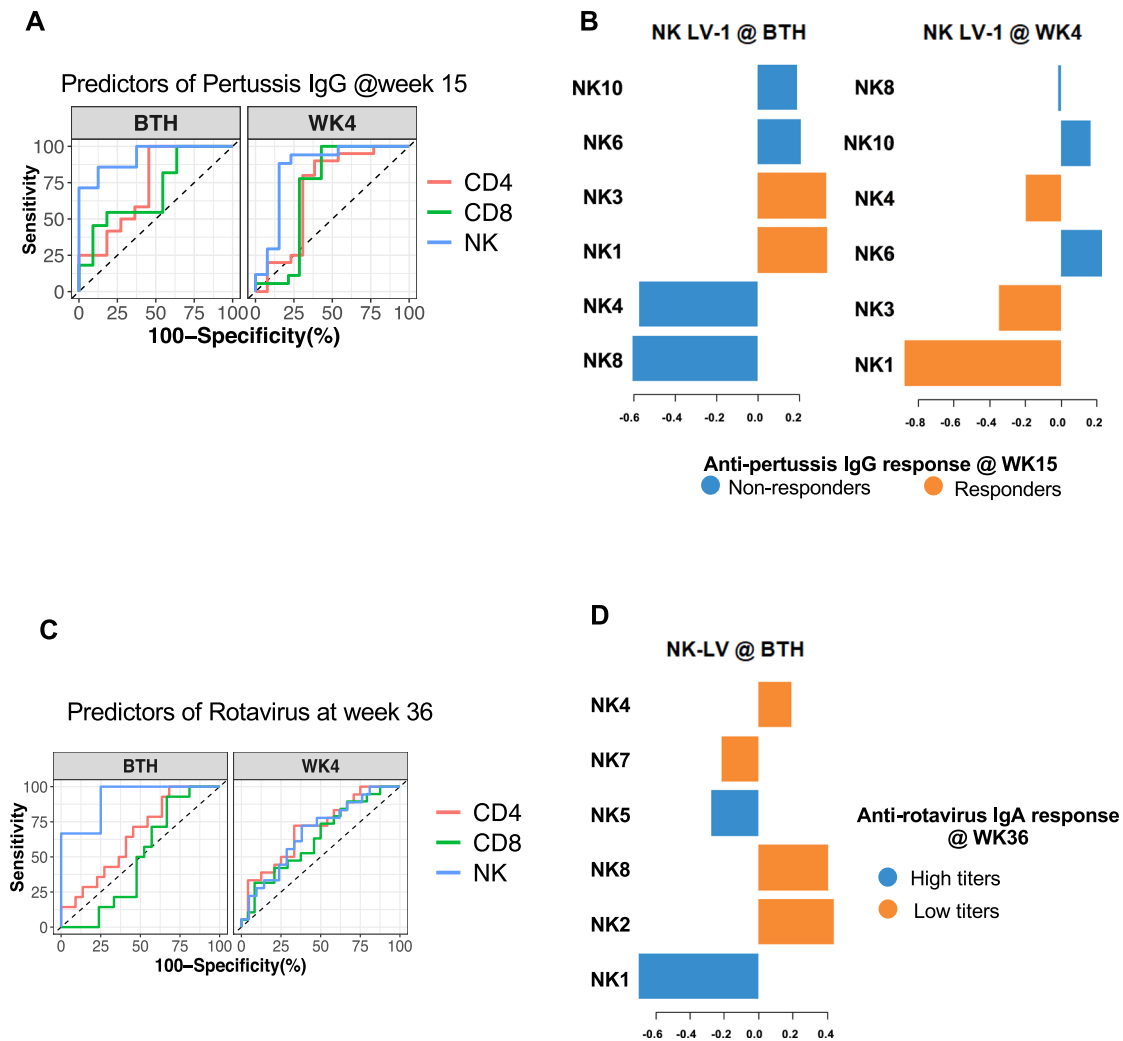


Fig. 5 | Early-life immune cell compositions predictive of antibody responses post-vaccination. **A, C** Summary of ROC analysis using the latent variable axis-1 derived from partial least square discriminate analysis (PLS-DA) of NK, CD4 and CD8 T cell clusters determined to be best predictors at birth and week 4 of pertussis

antibody responses at weeks 15 and rotavirus antibody response at week 36. **B, D** Loading variables from PLS-DA showing pre-vaccine cell clusters associated with good or poor antibody responses against pertussis and rotavirus vaccine at week 15 and 36 respectively. Sample size for each group is shown in Fig. S1.

(Fig. 5D). CD4⁺ or CD8⁺ T cell clusters were less accurate in predicting anti-rotavirus IgA response at week 36 (Fig. 5C, for CD4 clusters at birth: AUC = 0.65, $p = 0.13$; for CD8 clusters: AUC = 0.49, $p = 0.89$; at week 4: AUC = 0.7, $p = 0.027$; for CD8 clusters: AUC = 0.62, $p = 0.17$).

Collectively, these data show that specific NK cell phenotypes at birth, and in the first month of life, can predict vaccine-induced antibody responses to acellular pertussis and rotavirus at post-vaccination, regardless of infants being exposed to HIV. These data highlight the potential association between an early innate immune response with later T-cell dependent vaccine-induced antibody responses.

Discussion

Herein, we describe immune maturation in the first 9 months of life and how HIV/ARV exposure alters this ontological trajectory. Our findings show ordered immune changes during infancy, typical of the transition from innate-like and naïve neonatal immunity towards memory differentiated adaptive infant immunity^{30,41}. HIV exposure altered the immunological compositions of NK cells and T cells at different stages during infancy, with the T cell memory maturation being significantly impacted later in life. The impaired T cell memory maturation among iHEU could, in part, be due to diminished naïve TCR clonal pools observed in iHEU relative to iHUU. The skewing of TCR

clonality most likely initiated *in utero*, as differences between infant groups were observed as early as birth, as previously shown^{42,43}. We further showed that pre-vaccine NK cell composition could predict vaccine-induced antibody levels in infants better than T cells and is consistent with studies reporting baseline immunological signatures that are predictive of vaccine responses⁴⁴.

Although differentiated T cells are detected as early as 12–14 weeks in gestation^{45,46}, neonatal immunity is predominantly naïve and characterised by the abundance of CD45RA⁺ T cells⁷. T cell memory expansion during infancy is therefore essential in protecting against pathogens⁴⁷. Here we observed that the overall trajectory of T cell phenotypic composition in iHEU diverged from that of iHUU, particularly after week 15 of life. Both CD4⁺ and CD8⁺ T cell compartments in iHEU had lower frequencies of activated cells and memory differentiated cells expressing either PD-1 and/or perforin compared to iHUU. Although studies conducted before the wide adoption of perinatal ARV treatment reported heightened immune activation and/or exhaustion in iHEU^{48,49}, more recent studies have shown reduced or impaired memory T cells among iHEU compared to iHUU^{17,50–52}. Such T cell alterations were associated with poor responses to vaccines and/or increased hospitalisation^{50,51}. Other viral infections occurring during pregnancy such as SARS-Cov2 have also been documented to alter

infant immunity even in the absence of viral transmission^{53,54}. Although these studies were limited in examining the difference in cord blood, early viral exposure resulted in lower frequencies of TNF- α and IFN- γ producing T cells⁵³. Further longitudinal investigations are required to determine the impact of these early life cellular immune changes and their association to clinical outcomes later in life.

The differentiation of naïve T cells to different memory subsets are dependent on the TCR diversity of the naïve T cells in recognising the different pathogen derived antigens presented via major histocompatibility complex (MHC) molecules on antigen presenting cells¹⁰. The poor T cell memory differentiation observed in iHEU could therefore be due to reduced pool of naïve TCR clones. This is supported by the observed differences in naïve TCR β clonality between iHEU and iHUU being apparent from birth and correlated to the differentiated T cells preceding the period where impaired T cell memory differentiation was observed among iHEU.

Gabriel et al. reported lower TCR β clonality in the cord blood of iHEU⁴² implying clonal expansion occurring *in utero*, a phenomenon also observed in SARS-Cov2 exposed infants⁵⁴. Our data further revealed that the memory T cells were the main contributors of reduced TCR β diversity among iHEU compared to iHUU at birth. In addition to lower TCR β diversity at birth, iHEU also had altered V β gene usage, with several genes being used more frequently relative to iHiUU. When using GLIPH2^{37,38}, however, we could not detect any predicted antigen specificity enriched among iHEU including HIV-specific clones. This contrasted with earlier studies showing higher frequencies of HIV-1 specific clones⁴² and reactivity of T cells towards HIV proteins in iHEU⁵⁵. What was evident instead was that naïve CD4⁺ and CD8⁺ TCR β specificities in iHUU were enriched for clones targeting CMV, EBV and HCV antigens.

Since we obtained >95% purity after sorting for naïve and memory T cells, we regard this as minimal contamination of naïve T cells by memory T cells that could account for these enriched clones. It is possible that the abundance of naïve T cells compared to memory T cells in infant PBMC contributed to sampling bias resulting in enriched TCR clones amongst naïve T cells compared to the memory fraction. We also rationalised that since we did not include CD95 in our panel, we could not tease out stem cell-like memory T cells that would also express CD45RA and CCR7 similar to naïve cells and thus contribute to the observed outcome^{56–58}.

These scenarios, however, do not explain the lack of antigen specific TCR clonal enrichment among iHEU who exhibited skewed TCR clonality and V β gene usage. In addition, the length of CDR3 derived from these clones were typically short, a phenomenon common with neonatal TCR repertoire, and did not differ between iHEU and iHUU. Altogether, these observations possibly suggest non-antigen driven mechanisms that resulted in the loss of diversification of the iHEU TCR repertoire. Factors such as homeostatic proliferation under chronic maternal immune activation and proinflammatory milieu could give rise to virtual T cells^{59–61}, altered thymic selection since iHEU have been reported to have reduced thymic size relative to iHUU^{43,62}, or partially dysfunctional RAG system could contribute to iHEU having skewed TCR clonality. Since it is evident that reduced TCR diversity in iHEU is associated with impaired T cell memory differentiation and possibly increasing vulnerability to infection among iHEU⁵¹, further investigations are required to decipher the mechanism responsible for the skewed TCR clonality in iHEU.

To better understand how these alterations in iHEU immunity could impact immunological responses we measured antibody response to common childhood vaccines such as to pertussis and rotavirus. Previous studies have consistently demonstrated that although maternally derived vaccine specific antibodies in iHEU are lower at birth, following vaccination the concentrations tend to increase to similar levels to those of iHUU, and for other vaccines, such as acellular pertussis vaccine and pneumococcal conjugate vaccine

(PCV), where iHEU antibody levels even surpass that of iHUU, albeit with poor functionality⁶³. In our cohort we also observed a similar trend for anti-pertussis IgG levels being higher in iHEU compared to iHUU. Our data further revealed that among iHEU, vaccine-specific responses tend to have a high degree of variance compared to iHUU. This enabled us to classify infants either as “poor” or “good” vaccine responders, and therefore allowing us to show that, instead of T cells, the composition of NK cells pre-vaccination was superior in predicting vaccine-induced antibody responses post vaccination. This was consistent with other studies showing innate immune cells, including NK cells, being good baseline markers for predicting vaccine-induced antibody responses, albeit in adults^{44,64}. NK cells either negatively or positively regulate adaptive immunity, including promoting immunoglobulin isotype switching and enhancing antibody production^{65,66}. Here we show that the abundance of CD56^{lo}CD16^{lo}CD38⁺CD45RA⁺Fc ϵ R1y⁺ NK cell subset prior to immunisation resulted in a “good” vaccine-induced antibody responses. This may be in agreement with Cuapio et al., who identified a CD56^{lo}NKG2C⁺ NK subset whose frequency at baseline correlated with anti-SARS-Cov2 antibody titres post-vaccination⁶⁴. These data suggest: (a) that NK cell immunity may be important for vaccine-induced adaptive immunity and (b) induction of NK cells soon after birth could be an approach to enhance vaccine immunogenicity for childhood vaccines. Further mechanistic investigations are required to validate these observations.

The novelty of our study lies with the longitudinal follow-up of our infants and linking matched sample analysis, involving the ontogeny of T cells and NK cells from birth to 36 weeks of life and their relation to TCR β , with vaccine-induced immunity. Limitations of our study included sample availability and characterising phenotypic changes of NK and T cells with inference to immune function by determining associations with TCR usage and vaccine-induced antibodies. More detailed cellular immune function would be required to validate the phenotypic characterisation. A further limitation was the inability to tease out the effect of HIV from ARV exposure since all pregnant women living with HIV receive ARV treatment as a standard of care⁶⁷.

In conclusion, our data show that immunity during infancy is impacted by HIV/ARV exposure in a sequential manner, starting with altered T cell clonality followed by delayed T cell memory differentiation. Of particular importance, is the finding that TCR clonotypic diversity is significantly lower in iHEU, with altered clonality of memory T cells soon after birth, suggesting *in utero* “priming” and the lower TCR diversity among naïve T cells associated with delayed T cell effector memory formation in these children. Although HIV/ARV exposure had a subtle impact on the NK cell trajectory, the relatively more abundant NK cell cluster in iHEU occurring of early in life was predictive of higher vaccine-induced antibody responses, suggesting the importance of innate immunity in early-life vaccine responses. Lastly, we show here a comprehensive phenotypic view of early life immune changes in response to HIV/ARV exposure, where these changes may well be linked to the observed vulnerability of comorbidities in iHEU relative to iHUU.

Methods

Ethics statement

This research study complies with all relevant ethical regulations and was approved by the Human Research Ethics Committee (HREC) of University of Cape Town (HREC reference number 285/2012). All the women enrolled in the study provided signed informed consent for themselves and their respective infants.

Study cohort

We analysed infants who were delivered by mothers living with and without HIV infection who were enrolled prospectively from birth and followed up until 9 months of age as previously described (Table S2)⁶⁸. Briefly, pregnant women ≥ 18 years who recently delivered <12 h were

modelled using a logistic regression function. For each fitted curve the dilution which corresponds to a 40% response (ED_{40}), compared to the virus controls, was determined and reported as the neutralisation titer. The ED_{40} represents the titre of the serum against a given virus, which represents a 60% reduction in amount of virus.

Mass cytometry

Processing. Post CyTOF acquisition, the files were normalised using Premessa R package and target populations were manually gated using FlowJo software (version 10.5.3, TreeStar). The target populations with >1000 events were exported as FCS files for downstream analysis using R, an open-source statistical software⁷². All files for the target populations were transformed by applying inverse hyperbolic sine with a cofactor of 5 and subjected to doublet detection and removal using `computeDoubletDensity` from the `scDblFinder` package⁷³.

Dimensional reduction. Median marker expressions for each sample were used to compute Euclidean distance matrix to determine multi-dimensional scaling (MDS) coordinates using the `cmdscale` function in R. MDS analysis were used to visualise immune cell trajectories. Further, marker expression intensities were used to implement Uniform Manifold Approximation and Projection (UMAP) while preserving local density distribution for visualisation using `densMAP` function from the `denvis` R package⁷⁴.

Cell Clustering. High resolution clustering of the target cell populations was performed using FlowSOM algorithm and the resulting clusters grouped into metaclusters using `ConsensusClusterPlus` available in the `CATALYST` R package⁷⁵. The immune cell clusters were visualised using hierarchical clustering and UMAP embedding. Centred log-ratios of the relative abundance of the cell clusters per sample were determined and used in Principal Component Analysis (PCA) for assessing immune cell compositional differences.

TCR sequencing

Pre-processing of TCR sequencing data. Raw sequencing data was pre-processed by `pRESTO`⁷⁶. Briefly, reads with mean Phred quality scores less than 20 were discarded, UMIs were extracted from the first 10 bp of read 1, and primer sequences masked. Next, a single consensus sequence was constructed from reads sharing the same UMI barcode and paired-end consensus sequences assembled into a full-length TCR sequence. In the case of non-overlapping mate-pairs, the human TRB reference was used to properly space non-overlapping reads. After removal of duplicate sequences, full-length reads were aligned and clonotypes assembled using `MiXCR`^{77,78}.

T cell immune repertoire analysis. To perform quality control on our bulk TCR sequencing data, we removed samples where fewer than 10 clones were detected ($n = 44$ samples) and where more clones were detected than cells were sorted ($n = 18$ samples). This yielded a total of 861 samples for downstream analysis. The `immunarch` package⁷⁹ operating in the open-source statistical software R was used for all downstream immune repertoire analysis, including calculation of CDR3 β lengths and repertoire diversity by the Inverse Simpson index and richness using `Chao1`.

Identification and annotation of T cell specificity groups. The `GLIPH2` algorithm was used to establish T cell specificity groups, clusters of CDR3 sequences that are predicted to bind to the same antigen, by discovering groups of CDR3 β sequences that share either global or local motifs^{37,38}. To assign specificity annotations to identified CDR3 β sequence clusters, we adapted an approach described by ref. 80. Briefly, we collected human CDR3 β sequences with known specificity from `VDJdb` (<https://vdjdb.cdr3.net/>) and identified CDR3 β sequences within this database that could form TCR specificity groups.

From 47,107 CDR3 β sequences, this process identified 11,648 specificity groups comprised of 25,759 unique CDR3 β sequences. We next combined these 25,759 annotated sequences with 108,183 unique experimental CDR3 β sequences from our bulk TCR repertoire profiling cohort. This was performed separately for CD4 and CD8 T, as there are differences between gene usage frequencies between CD4 and CD8 T cells that can impact specificity predictions. We prioritised TCR specificity groups with at least 3 distinct CDR3 β sequences. This process yielded 17,154 CDR3 β sequences in 11,629 specificity groups for CD4 T cells, and 15,107 CDR3 β sequences in 9911 specificity groups for CD8 T cells.

Statistical analysis

All statistical analysis and graphical visualisation of the data was performed on the open R software⁷². Spearman's rank correlation was used to test for the correlations between the frequencies of the cell clusters with either infant age or antibody responses and p values adjusted for multiple comparisons using false discovery rates (FDR). To compare differences in the abundance of cell clusters between iHEU and iHUU the generalised linear model from the `diffcyt` package was used⁸¹. Pairwise comparisons of medians between groups were performed using Wilcoxon-rank test or Kruskal-Wallis for multiple group comparisons and the p values adjusted for multiple comparisons using Benjamin Hochberg correction. To determine cell clusters that were predictive of antibody responses following vaccination, we used the multivariate modelling algorithm from `MUVR` package that incorporates recursive variable selection using repeated double cross-validation within partial least squares modelling⁴⁰.

Reporting summary

Further information on research design is available in the Nature Portfolio Reporting Summary linked to this article.

Data availability

FCS files for CyTOF data that was used for analysing infant immune trajectories and FACS data generated when sorting for naïve and memory CD4+ and CD8+ T cells are available at ImmPort repository (study accession [SDY2463](#)). FASTQ files generated from TCR RNA sequencing are available at Gene Expression Omnibus (accession [GSE256410](#)) The data files used for quantification of vaccine-specific antibody responses are available at [Figshare](#) repository. Source data are provided with this paper.

References

1. Perin, J. et al. Global, regional, and national causes of under-5 mortality in 2000–19: an updated systematic analysis with implications for the Sustainable Development Goals. *Lancet Child Adolesc. Health* **6**, 106–115 (2022).
2. Zimmermann, P. & Jones, C. E. Factors that influence infant immunity and vaccine responses. *Pediatr. Infect. Dis. J.* **40**, S40–S46 (2021).
3. Pasetti, M. F. et al. Maternal determinants of infant immunity: implications for effective immunization and maternal-child health. *Vaccine* **38**, 4491–4494 (2020).
4. Sanidad, K. Z. & Zeng, M. Y. Neonatal gut microbiome and immunity. *Curr. Opin. Microbiol.* **56**, 30–37 (2020).
5. Goenka, A. & Kollmann, T. R. Development of immunity in early life. *J. Infect.* **71**, S112–S120 (2015).
6. Aagaard, K. et al. The placenta harbors a unique microbiome. *Sci. Transl. Med.* **6**, 229–262 (2014).
7. Tosato, F. et al. Lymphocytes subsets reference values in childhood. *Cytom. Part A* **87**, 81–85 (2015).
8. Howie, P. W., Forsyth, J. S., Ogston, S. A., Clark, A. & Du Florey, V. C. Protective effect of breast feeding against infection. *Br. Med. J.* **300**, 11–16 (1990).

9. Sankar, M. J. et al. Optimal breastfeeding practices and infant and child mortality: a systematic review and meta-analysis. *Acta Paediatr. Int. J. Paediatr.* **104**, 3–13 (2015).
10. Nikolich-Zugich, J., Slifka, M. K. & Messaoudi, I. The many important facets of T-cell repertoire diversity. *Nat. Rev. Immunol.* **4**, 123–132 (2004).
11. Anderson, K. et al. Increased infectious-cause hospitalization among infants who are HIV-exposed uninfected compared with HIV-unexposed. *AIDS* **35**, 2327–2329 (2021).
12. Brennan, A. T. et al. A meta-analysis assessing all-cause mortality in HIV-exposed uninfected compared with HIV-unexposed uninfected infants and children. *Aids* **30**, 2351–2360 (2016).
13. Cohen, C. et al. Epidemiology of acute lower respiratory tract infection in HIV-Exposed Uninfected Infants. *Pediatrics* **137**, e20153272 (2016).
14. Slogrove, A. L., Goetghebuer, T., Cotton, M. F., Singer, J. & Bettinger, J. Pattern of infectious morbidity in HIV-exposed uninfected infants and children. *Front. Immunol.* **7**, 1–8 (2016).
15. Brennan, A. T. et al. A meta-analysis assessing diarrhea and pneumonia in HIV-exposed uninfected compared to HIV-unexposed uninfected infants and children. *JAIDS J. Acqui. Immune Defic. Syndr.* **82**, 1–8 (2019).
16. Slogrove, A. L., Powis, K. M., Johnson, L. F., Stover, J. & Mahy, M. Estimates of the global population of children who are HIV-exposed and uninfected, 2000–18: a modelling study. *Lancet Glob. Health* **8**, e67–e75 (2020).
17. Dzanibe, S. et al. Stereotypic expansion of T regulatory and Th17 cells during infancy is disrupted by HIV Exposure and gut epithelial damage. *J. Immunol.* **208**, 27–37 (2022).
18. Uksila, J., Lassila, O. & Hirvonen, T. Natural killer cell function of human neonatal lymphocytes. *Clin. Exp. Immunol.* **48**, 649–654 (1982).
19. Choi, S. S. et al. Interleukin-15 enhances cytotoxicity, receptor expression, and expansion of neonatal natural killer cells in long-term culture. *Clin. Diagn. Lab Immunol.* **11**, 879–888 (2004).
20. Xing, D. et al. Cord blood natural killer cells exhibit impaired lytic immunological synapse formation that is reversed with il-2 ex vivo expansion. *J. Immunother.* **33**, 684–696 (2010).
21. Strauss-Albee, D. M., Liang, E. C., Ranganath, T., Aziz, N. & Blish, C. A. The newborn human NK cell repertoire is phenotypically formed but functionally reduced. *Cytom. B Clin. Cytom.* **92**, 33–41 (2017).
22. Smith, C. et al. Altered natural killer cell function in HIV-exposed uninfected infants. *Front. Immunol.* **8**, 1–13 (2017).
23. Slyker, J. A. et al. The impact of HIV-1 infection and exposure on natural killer (NK) cell phenotype in Kenyan infants during the first year of life. *Front. Immunol.* **3**, 1–16 (2012).
24. Vilches, C. & Parham, P. KIR: Diverse, rapidly evolving receptors of innate and adaptive immunity. *Annu. Rev. Immunol.* **20**, 217–251 (2002).
25. Sun, J. C., Beilke, J. N. & Lanier, L. L. Adaptive immune features of natural killer cells. *Nature* **457**, 557–561 (2009).
26. Muntasell, A., Magri, G., Pende, D., Angulo, A. & López-Botet, M. Inhibition of NKG2D expression in NK cells by cytokines secreted in response to human cytomegalovirus infection. *Blood* **115**, 5170–5179 (2010).
27. Flommersfeld, S. et al. Fate mapping of single NK cells identifies a type 1 innate lymphoid-like lineage that bridges innate and adaptive recognition of viral infection. *Immunity* **54**, 2288–2304.e7 (2021).
28. Bunis, D. G. et al. Single-cell mapping of progressive fetal-to-adult transition in human naive T Cells. *Cell Rep.* **34**, 108573 (2021).
29. Singh, A. et al. DIABLO: an integrative approach for identifying key molecular drivers from multi-omics assays. *Bioinformatics* **35**, 3055–3062 (2019).
30. Simon, A. K., Hollander, G. A. & McMichael, A. Evolution of the immune system in humans from infancy to old age. *Proc. R. Soc. B: Biol. Sci.* **282**, 20143085 (2015).
31. Larbi, A. & Fulop, T. From ‘truly naïve’ to ‘exhausted senescent’ T cells: When markers predict functionality. *Cytom. Part A* **85**, 25–35 (2014).
32. Takeuchi, A. & Saito, T. CD4 CTL, a cytotoxic subset of CD4⁺ T cells, their differentiation and function. *Front. Immunol.* **8**, 194 (2017).
33. Peralbo, E., Alonso, C. & Solana, R. Invariant NKT and NKT-like lymphocytes: two different T cell subsets that are differentially affected by ageing. *Expe. Gerontol.* **42**, 703–708 (2007).
34. Wilk, A. J. & Blish, C. A. Diversification of human NK cells: Lessons from deep profiling. *J. Leukoc. Biol.* **103**, 629–641 (2018).
35. Chikuma, S. et al. PD-1-Mediated Suppression of IL-2 Production Induces CD8⁺ T Cell Energy In Vivo. *J. Immunol.* **182**, 6682–6689 (2009).
36. Petrovas, C. et al. PD-1 is a regulator of virus-specific CD8⁺ T cell survival in HIV infection. *J. Exp. Med.* **203**, 2281–2292 (2006).
37. Glanville, J. et al. Identifying specificity groups in the T cell receptor repertoire. *Nature* **547**, 94–98 (2017).
38. Huang, H., Wang, C., Rubelt, F., Scriba, T. J. & Davis, M. M. Analyzing the Mycobacterium tuberculosis immune response by T-cell receptor clustering with GLIPH2 and genome-wide antigen screening. *Nat. Biotechnol.* **38**, 1194–1202 (2020).
39. Walker, J. A. & McKenzie, A. N. J. TH2 cell development and function. *Nat. Rev. Immunol.* **18**, 121–133 (2018).
40. Shi, L., Westerhuis, J. A., Rosén, J., Landberg, R. & Brunius, C. Variable selection and validation in multivariate modelling. *Bioinformatics* **35**, 972–980 (2019).
41. Olin, A. et al. Stereotypic immune system development in newborn children. *Cell* **174**, 1277–1292.e14 (2018).
42. Gabriel, B. et al. Analysis of the TCR Repertoire in HIV-Exposed but Uninfected Infants. *Sci. Rep.* **9**, 11954 (2019).
43. Kolte, L. et al. Reduced thymic size but no evidence of impaired thymic function in uninfected children born to human immunodeficiency virus-infected mothers. *Pediatr. Infect. Dis. J.* **30**, 325–330 (2011).
44. Hagan, T. et al. Transcriptional atlas of the human immune response to 13 vaccines reveals a common predictor of vaccine-induced antibody responses. *Nat. Immunol.* **23**, 1788–1798 (2022).
45. Haynes, B. Y. B. E., Martin, M. E., Kay, H. H. & Kurtzberg, J. Early events in human T cell ontogeny. Phenotypic characterization and immunohistologic localization of T cell precursors in early human fetal tissues. *J. Exp. Med.* **168**, 1061–1080 (1988).
46. Haynes, B. F. & Heinly, C. S. Early human T cell development: analysis of the human thymus at the time of initial entry of hematopoietic stem cells into the fetal thymic microenvironment. *J. Exp. Med.* **181**, 1445–1458 (1995).
47. Scheible, K. M. et al. T cell developmental arrest in former premature infants increases risk of respiratory morbidity later in infancy. *JCI Insight* **3**, e96724 (2018).
48. Rich, K. C., Siegel, J. N., Jennings, C., Rydman, R. J. & Landay, A. L. Function and phenotype of immature CD4⁺ lymphocytes in healthy infants and early lymphocyte activation in uninfected infants of human immunodeficiency virus-infected mothers. *Clin. Diagn. Lab Immunol.* **4**, 358–361 (1997).
49. Ono, E. et al. Imbalance of naive and memory T lymphocytes with sustained high cellular activation during the first year of life from uninfected children born to HIV-1-infected mothers on HAART. *Braz. J. Med. Biol. Res.* **41**, 700–708 (2008).
50. Garcia-Knight, M. A. et al. Altered memory T-cell responses to Bacillus Calmette-Guerin and Tetanus Toxoid vaccination and altered cytokine responses to polyclonal stimulation in HIV-exposed uninfected Kenyan infants. *PLoS One* **10**, 1–19 (2015).
51. Smith, C. et al. Human immunodeficiency virus exposure but not early cytomegalovirus infection is associated with increased hospitalization and decreased memory T-Cell responses to tetanus vaccine. *J. Infect. Dis.* **221**, 1167–1175 (2020).

52. Pérez, Y. B. et al. Impaired T helper cell responses in human immunodeficiency virus - exposed uninfected newborns. *Inflamm. Dis.* **9**, 1541–1553 (2021).
53. Gee, S. et al. The legacy of maternal SARS-CoV-2 infection on the immunology of the neonate. *Nat. Immunol.* **22**, 1490–1502 (2021).
54. Matute, J. D. et al. Single-cell immunophenotyping of the fetal immune response to maternal SARS-CoV-2 infection in late gestation. *Pediatr. Res.* **91**, 1090–1098 (2022).
55. Holditch, S. J. et al. Decay kinetics of HIV-1 specific cell responses in vertically HIV-1 exposed seronegative infants. *Front. Immunol.* **2**, 1–6 (2012).
56. Pušnik, J. et al. Expansion of stem Cell-Like CD4 + Memory T cells during acute HIV-1 infection is linked to rapid disease progression. *J. Virol.* **93**, e00377–19 (2019).
57. Ribeiro, S. P. et al. The CD8 + Memory Stem T Cell (T SCM) Subset Is Associated with Improved Prognosis in Chronic HIV-1 Infection. *J. Virol.* **88**, 13836–13844 (2014).
58. Gattinoni, L. et al. A human memory T cell subset with stem cell-like properties. *Nat. Med.* **17**, 1290–1297 (2011).
59. Savid-Frontera, C. et al. Exploring the immunomodulatory role of virtual memory CD8+ T cells: role of IFN gamma in tumor growth control. *Front. Immunol.* **13**, 1–18 (2022).
60. Lee, J. Y., Hamilton, S. E., Akue, A. D., Hogquist, K. A. & Jameson, S. C. Virtual memory CD8 T cells display unique functional properties. *Proc. Natl Acad. Sci. USA* **110**, 13498–13503 (2013).
61. Rolot, M. et al. Helminth-induced IL-4 expands bystander memory CD8+ T cells for early control of viral infection. *Nat. Commun.* **9**, 4516 (2018).
62. Nielsen, S. D. et al. Impaired progenitor cell function in HIV-negative infants of HIV-positive mothers results in decreased thymic output and low CD4 counts. *Blood.* **98**, 398–404 (2001).
63. Falconer, O., Newell, M. L. & Jones, C. E. The effect of human immunodeficiency virus and Cytomegalovirus infection on infant responses to vaccines: a review. *Front. Immunol.* **9**, 328 (2018).
64. Cuapio, A. et al. NK cell frequencies, function and correlates to vaccine outcome in BNT162b2 mRNA anti-SARS-CoV-2 vaccinated healthy and immunocompromised individuals. *Mol. Med.* **28**, 20 (2022).
65. Rydzynski, C. E. & Waggoner, S. N. Boosting vaccine efficacy the natural (killer) way. *Trends Immunol.* **36**, 536–546 (2015).
66. Rydzynski, C. E. et al. Affinity maturation is impaired by natural killer cell suppression of germinal centers. *Cell Rep.* **24**, 3367–3373.e4 (2018).
67. Wessels, J. et al. The updated South African National Guideline for the Prevention of Mother to Child Transmission of Communicable Infections (2019). *South Afr. J. HIV Med.* **21**, 1–8 (2020).
68. Tchakoute, C. T. et al. Breastfeeding mitigates the effects of maternal HIV on infant infectious morbidity in the Option B+ era. *AIDS* **32**, 2383–2391 (2018).
69. Vendrame, E. et al. Profiling of the Human Natural Killer Cell Receptor-Ligand Repertoire. *J. Visualized Exp.* **165**, 139–148 (2020).
70. Rubelt, F. et al. Individual heritable differences result in unique cell lymphocyte receptor repertoires of naïve and antigen-experienced cells. *Nat. Commun.* **7**, 1–12 (2016).
71. Knowlton, D. R., Spector, D. M. & Ward, R. L. Development of an improved method for measuring neutralizing antibody to rotavirus. *J. Virol. Methods* **33**, 127–134 (1991).
72. RCoreTeam. R: A language and environment for statistical computing. R Foundation for Statistical Computing, Vienna, Austria. <https://www.R-project.org/>
73. Germain, P.-L., Lun, A., Garcia Meixide, C., Macnair, W. & Robinson, M. D. Doublet identification in single-cell sequencing data using scDblFinder. *F1000Res* **10**, 979 (2022).
74. Narayan, A., Berger, B. & Cho, H. Assessing single-cell transcriptomic variability through density-preserving data visualization. *Nat. Biotechnol.* **39**, 765–774 (2021).
75. Nowicka, M. et al. CyTOF workflow: differential discovery in high-throughput high-dimensional cytometry datasets. *F1000Res.* **6**, eCollection (2017).
76. Vander Heiden, J. A. et al. PRESTO: a toolkit for processing high-throughput sequencing raw reads of lymphocyte receptor repertoires. *Bioinformatics* **30**, 1930–1932 (2014).
77. Bolotin, D. A. et al. MiXCR: Software for comprehensive adaptive immunity profiling. *Nat. Methods* **12**, 380–381 (2015).
78. Bolotin, D. A. et al. Antigen receptor repertoire profiling from RNA-seq data. *Nat. Biotechnol.* **35**, 908–911 (2017).
79. ImmunoMind Team. immunarch: An R Package for Painless Bioinformatics Analysis of T-Cell and B-Cell Immune Repertoires. *Zenodo* <https://doi.org/10.5281/zenodo.3367200> (2019).
80. Chiou, S. H. et al. Global analysis of shared T cell specificities in human non-small cell lung cancer enables HLA inference and antigen discovery. *Immunity* **54**, 586–602.e8 (2021).
81. Weber, L. M. diffcyt: Differential discovery in high-dimensional cytometry via high-resolution clustering. *Commun Biol.* **13**, eCollection1 (2019).

Acknowledgements

We would like to acknowledge the technical staff that assisted in the completion of this study. This includes Euan Johnston, Emily Tangie and Carine Kilola who assisted with the CyTOF experiments, Mikayla Stabile, Michelle Leong, Cassandra Pinedo, and Nicole Prins, for assistance with TCR RNA-seq processing, Llyod Leach for assistance with measuring pertussis antibody responses and Monica McNeal for measuring rotavirus antibody responses. This work was supported by the Eunice Kennedy Shriver National Institute of Child Health and Human Development, National Institutes of Health R01HD102050 awarded to C.M.G. and H.B.J., and U01AI131302 to C.A.B., C.M.G. and H.B.J., and Fogarty International Training Center (D71TW012265) to C.M.G. and South African Medical Research Council (SA-MRC) to S.D. S.D. was supported by the Wellcome Trust International Training Fellowship (221995/Z/20/Z).

Author contributions

Conceived by C.M.G., C.A.B., and H.B.J., Method set-up and validation by S.D., A.W., S.C., T.R., F.R., H.H., and M.D. Study participant enrolment, sample collection and processing by H.B.J. and B.A. Experimental investigations by S.D. Data and statistical analysis by S.D., A.W., and S.P.H. Original draft by S.D. Reviewed and edited by all authors.

Competing interests

The authors declare no competing interests.

Additional information

Supplementary information The online version contains supplementary material available at <https://doi.org/10.1038/s41467-024-47955-5>.

Correspondence and requests for materials should be addressed to Heather B. Jaspan, Catherine A. Blish or Clive M. Gray.

Peer review information *Nature Communications* thanks Kristina De Paris, Deena Gibbons and the other, anonymous, reviewer(s) for their contribution to the peer review of this work. A peer review file is available.

Reprints and permissions information is available at <https://www.nature.com/reprints>

Publisher's note Springer Nature remains neutral with regard to jurisdictional claims in published maps and institutional affiliations.

Open Access This article is licensed under a Creative Commons Attribution 4.0 International License, which permits use, sharing, adaptation, distribution and reproduction in any medium or format, as long as you give appropriate credit to the original author(s) and the source, provide a link to the Creative Commons licence, and indicate if changes were made. The images or other third party material in this article are included in the article's Creative Commons licence, unless indicated otherwise in a credit line to the material. If material is not included in the article's Creative Commons licence and your intended use is not permitted by statutory regulation or exceeds the permitted use, you will need to obtain permission directly from the copyright holder. To view a copy of this licence, visit <http://creativecommons.org/licenses/by/4.0/>.

© The Author(s) 2024